Local Structure and Dynamics of *trans*-Polyisoprene Oligomers

Roland Faller,*,† Florian Müller-Plathe,† Manolis Doxastakis,‡ and Doros Theodorou‡

Max-Planck-Institut für Polymerforschung, Ackermannweg 10, D-55128 Mainz, Germany, and Department of Chemical Engineering, University of Patras and ICE/HT-FORTH, GR-26500 Patras, Greece

Received September 26, 2000; Revised Manuscript Received December 26, 2000

ABSTRACT: Mono- and polydisperse melts of oligomers (average length 10 monomers) of *trans*-1,4-polyisoprene are simulated in full atomistic detail. The force field is developed by means of a mixture of ab initio quantum chemistry and an automatic generation of empirical parameters. Comparisons to NMR and scattering experiments validate the model. The local reorientation dynamics shows that for C−H vectors there is a two-stage process consisting of an initial decay and a late-stage decorrelation originating from overall reorientation. The atomistic model can be successfully mapped onto a simple model including only beads for the monomers with bond springs and bond angle potentials. End-bridging Monte Carlo as an equilibration stage and molecular dynamics as the subsequent simulation method together prove to be a useful method for polymer simulations.

1. Introduction

The understanding of polymer materials from the very local to the macroscopic scale is at the focus of theoretical material science. Simulations are a useful means for reaching this goal. Fully detailed simulations incorporating interaction centers for all atoms allow extensive investigations of polymer-specific models to compare directly to high-resolution experiments like neutron scattering,[1] positronium annihilation spectroscopy,[2] or nuclear magnetic resonance.[3] In contrast to simple generic models,[4] atomistic simulations capture the differences between polymer species. This understanding is a prerequisite for the design of tailor-made materials for special applications.

The present contribution investigates, as an example, oligomers of *trans*-1,4-polyisoprene. We focus on *local* structure and dynamics as the local scale is influenced mainly by the specific chemical structure. In this range all-atom models are necessary for a reliable static and dynamic investigation.[5] Moreover, we compare our results to NMR measurements, which always sample atom−atom vectors. Therefore, it is useful for the analysis to have all atoms present. For the properties under investigation short chains are sufficient, as the connectivity and noncrossability contribute to phenomena on the generic large-scale level[6,7] which is not of interest here. Several experiments have been performed aimed at the local properties of polyisoprene like reorientation times and the packing.[8−13] Additionally, simulations of pure *cis*-polyisoprene are already known.[1,14] To our knowledge there are, however, not yet simulations of the trans conformer. Industrially, this conformer is not as important as the cis conformer. However, typical polyisoprene materials include several percent trans content. To understand the influence of this content, it is worth investigating pure *trans*-polyisoprene and look for differences from the other conformers.

† Max-Planck-Institut für Polymerforschung.
‡ University of Patras and ICE/HT-FORTH.
* Corresponding author. New address: Department of Chemical Engineering, University of Wisconsin, Madison, WI 53706.

Table 1. Nonbonded Parameters (Lennard-Jones 12−6) Used in the United Atom End-Bridging Monte Carlo Simulations of *trans*-Polyisoprene[a]

interaction	σ [nm]	ϵ [kJ/mol]
C−C, C−CH, CH−CH	0.38	0.4186
C−CH_2, CH−CH_2	0.4257	0.4249
C−CH_3, CH−CH_3	0.4257	0.6299
CH_2−CH_2	0.45	0.3918
CH_2−CH_3	0.45	0.6095
CH_3-CH_3	0.45	0.9479

[a] Bond lenghts, angles, and torsion potentials are the same as in the all-atom simulations. All interactions within a topological distance of up to three bonds are excluded, as they are taken into account in the torsion potentials

2. The Simulation Model and Technical Details

2.1. Starting Structures from Quantum Chemistry. Three different chain length mixtures, each containing 100 oligomers (13 200 atoms) of polyisoprene with an average molecular weight of 682 g/mol (corresponding to 10 monomers), are simulated at temperatures of 300 and 413 K. One system is monodisperse (in the following referred to as system 1) and is simulated at constant density of 890 kg/m^3 (experimental density of the cis conformer: 900 kg/m^3)[15] in an orthorhombic box under periodic boundary conditions with box lengths 4.97 nm × 5.16 nm × 4.97 nm. This is about $2^1/_2$ times the end-to-end distance of the chains; thus, artifacts from interactions of chains with their mirror images are absent. The torsional conformations were set up in the equilibrium distribution derived from quantum chemical calculations. Twenty-seven configurations of a dimer were investigated with quantum chemical calculations (for details see section 2.3). Only seven of them are actually at low energy (Table 3), and only their statistics was used to generate initial torsional distributions. The chains were packed in a simulation box of 9 nm × 9 nm × 9 nm and compressed to the final density in steps, using molecular dynamics. During this procedure anisotropic box fluctuations were allowed to better equilibrate stresses in the box leading to the orthorhombic box explained above. At the same time the time step was increased from 0.01 to 1 fs.

10.1021/ma0016782 CCC: $20.00
Published on Web 02/01/2001

Table 2. Force Field Parameters for the Torsion Angles; For the Nomenclature See Figure 1

torsion	dihedral angle τ_0 [deg]	strength k_τ [kJ/mol]	periodicity i
1	0	5.2	1
1	0	-7.4	2
1	0	10.0	3
2	180	9.7	1
2	180	14.1	3
3	0	-21.1	1
3	0	-12.3	2
3	0	0.5	3

Table 3. Relevant Torsion Conformations after Geometry Optimizations Using the Hybrid Method 6-311G/B3LYP**

conf	torsion 1 $C_2-C_3-C_5-C_1$	torsion 2 $C_3-C_5-C_1-C_2$	torsion 3 $C_5-C_1-C_2-C_3$	ΔE [kJ/mol]
1	180.0	180.0	180.0	42.56
2	−111.2	176.1	115.7	0.33
3	117.4	−62.9	133.5	2.87
4	115.3	−63.8	−124.0	2.28
5	−109.3	−177.7	−115.3	0.00
6	−94.9	−70.5	123.6	4.91
7	−86.0	−59.0	−108.3	6.72

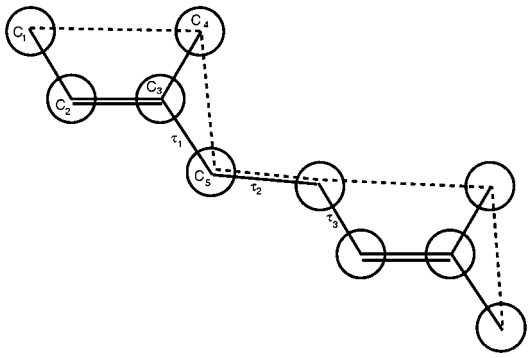

Figure 1. Carbons in the dimer of *trans*-polyisoprene with definition of the torsions. Additionally, the hypothetical chain for the end-bridging moves is shown as a dashed line.

2.2. Starting Structure via End-Bridging Monte Carlo. The two polydisperse systems (systems 2 and 3) were additionally equilibrated using the end-bridging Monte Carlo (EBMC) procedure[16,17] before the molecular dynamics simulations were performed at a constant pressure of 101.3 kPa to determine the density in a polydisperse melt. We used two systems with slightly different chain length distributions (see below) in order to increase the statistics and to look for influences of the actual realization of the ensemble.

The EBMC was performed in a united-atom model as the positions of the hydrogens are not important at this stage. The nonbonded interaction potential parameters for this procedure are shown in Table 1. All Monte Carlo steps are accepted according to the Metropolis criterion.

The end-bridging steps were performed using a hypothetical chain (see dashed line in Figure 1). The monomers on this chain consist only of the carbons 1, 4, and 5. Unlike the original procedure for polyethylene,[16,17] moves can only be performed breaking the bonds between carbon 5 and 1 as the topology of *trans*-polyisoprene must not be altered. As the bridging procedure always needs three trimers—one to bridge from, one to bridge to, and one as the bridge—the three carbons of one pseudo-monomer act as such trimers. After the respective move the positions of carbons 2 and 3 have to be recalculated. Since the double bond keeps

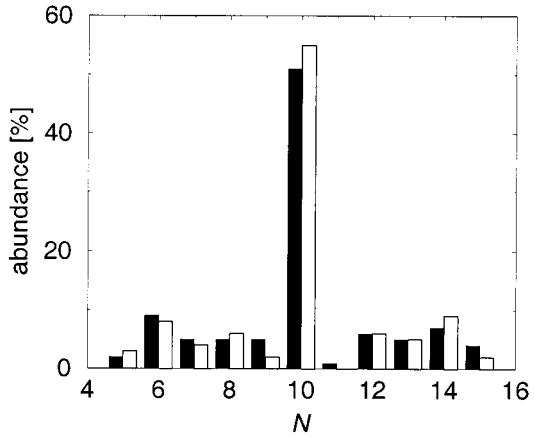

Figure 2. Molecular weight distributions of systems 2 (filled bars) and 3 (open bars)

the whole monomer in plane, the positions are defined exactly if bond lengths and angles are left unchanged. In the Monte Carlo procedure no bond length or bond angle was changed, neither for the hypothetical chain nor for the atomistic chain. Any of these local degrees of freedom were left for the molecular dynamics to equilibrate. Anisotropic box fluctuations were allowed but no shearing. The systems are slightly polydisperse, as this version of EBMC does not work at constant topology, i.e., chain length distribution. The molecular weight distribution is sharply peaked at $N = 10$ (Figure 2) as we did not intend to equilibrate the chain length distribution but to investigate nearly monodisperse systems. We started with a monodisperse sample and let the end-bridging procedure run for a limited time with chemical potential $\mu = 0$ for $5 \leq N \leq 15$ and $\mu = -\infty$ elsewhere. Strict monodispersity, however, would require much longer equilibration times as EBMC would be prohibited. On average, every chain underwent 2.8 successful end-bridging moves in addition to many local moves before the molecular dynamics started. The resulting distribution shows two weak side peaks at $N \approx 6$ and $N \approx 14$. These can be explained by the procedure. Chain lengths of 9 or 11 are not directly accessible by end-bridging moves starting from the initial monodisperse ($N = 10$) sample, as no single monomers can be transferred. Since they have to be reached indirectly, they have a low probability.

2.3. The Force Field. As the torsion potentials are very important for the configurations of the chains, quantum chemical calculations were performed with the packages Gaussian 94[18] and Gaussian 98.[19] The energy differences between different minima were calculated with hybrid density functional calculations (B3LYP),[20] and the barrier heights are calculated by Hartree−Fock using a 6-31G** basis set on a dimer of *trans*-polyisoprene. To calculate barrier heights, constrained optimizations at fixed bond lengths are applied where the torsions are changed in steps of 15° or 30°. The results were fitted to a Fourier series in the torsion angle with four terms. The constant energy shift is discarded as it does not enter the forces

$$V_{\text{tors}} = \sum_{i=1}^{3} k_\tau/2[1 - \cos[i(\tau - \tau_0)]] \qquad (1)$$

The resulting parameters are shown in Table 2. The relevant minima are first supposed to occur in trans and

Table 4. Angles and Bond Lengths for Atomistic Simulations[a]

angle	ϕ_0	k [kJ/(mol rad^2)]	bond	l_b [nm]
$C_1-C_2-C_3$	128.7	250	C_1-C_2	0.150
$C_2-C_3-C_4$	124.4	250	$C_1=C_2$	0.1338
$C_2-C_3-C_5$	120.2	250	C_3-C_4	0.151
$C_4-C_3-C_5$	115.4	250	C_3-C_5	0.1515
$C_3-C_5-C_1$	114.5	250	C_5-C_1	0.155
$C_5-C_1-C_2$	112.7	250	C−H	0.109
$C-C_{sp^3}-H$	109.5	250		
C_1-C_2-H	114.4	250		
C_3-C_2-H	114.4	250		
H−C−H	109.5	250		

[a] The equilibrium values of the angles ϕ_0 and the bond lengths l_b are derived from density functional calculations using Gaussian 94[18] and experimental data;[46] k is the force constant for the harmonic bond angle potential. The bond lengths are constrained.

Table 5. Force-Field Parameters for the Nonbonded Interactions[a]

atom	m [amu]	σ [nm]	ϵ [kJ/mol]
C_{sp^2}	12.01	0.321	0.313
C_{sp^3}	12.01	0.311	0.313
H	1.00782	0.24	0.2189

[a] m is the atom mass, σ the interaction radius, and ϵ the interaction strength.

gauche states. The initial torsion states are set up according to this distribution (before EBMC) in a Markov chain way; i.e., the chains are built monomer by monomer, and the triple of torsions connecting two monomers is selected by random numbers according to the energy distribution.

The bond angle potential and the improper dihedral potential, which keeps the atoms at the double bond in plane, are harmonic with force constants adapted from previous simulations of small molecules (Table 4).[21,22] The harmonic dihedral has a strength of 160 kJ/(mol rad^2) and is applied to the dihedrals $C_1-C_2-C_3-C_4$, $H_{C2}-C_2-C_3-C_5$, and $C_2-C_3-C_4-C_5$. Also, the nonbonded interaction parameters (Table 5) are adapted from simulations of cyclohexene.[22] They were derived using the automatic simplex parametrization.[21] The polymer density was not fully satisfactory with the original cyclohexene force field.[23] Thus, the σ value of the hydrogens was slightly increased to reproduce the experimental density at 300 K. Lennard-Jones interactions between unlike atoms were based on the Lorentz−Berthelot mixing rules.[24]

Atoms connected by any bonding potential did not interact by the Lennard-Jones potential. Additionally, the following nonbonded interactions were excluded: all within one monomer and all C−C, C−H, and H−H interactions between the second half of the carbons of one monomer (atoms C_3, C_4, and C_5) and the first half of its following neighbor (C_1 and C_2) including the hydrogens connected to them for system 1. For system 2 and 3 the latter C−H and H−H interactions were not excluded (only up to "1-4" interactions), which leads to differences as the different torsion states alter the distances between these atoms so that the effective energies of the torsions are shifted. This happened due to an oversight in the initial simulations. As the simulations are very time-consuming, we deemed a complete repetition not necessary.

Constant temperature and pressure are ensured using Berendsen's method[25] with time constants 0.2 ps for temperature and 8 ps (system 2) or 12 ps (system 3) for pressure, respectively. The pressure coupling using a compressibility of 2×10^{-7} kPa^{-1} was employed for the three directions independently. All simulations were performed using the YASP molecular simulation package[26] with a time step of 1 fs and a cutoff for the nonbonded interactions at 0.9 nm. Configurations were saved every picosecond. Simulation lengths and polydispersities are shown in Table 6. Bond lengths are constrained to the desired values of Table 4 using the SHAKE algorithm.[27,28]

Table 6. Simulation Parameters for the Three Systems under Study[a]

system	T [K]	t_{sim} [ps]	M_w/M_n	ρ [kg/m^3]
1	300	1184	1.00	890
2	300	2012	1.05	917.4
3	300	1737	1.05	916.8
3	413	792	1.05	826

[a] Before the above-mentioned simulation time was started a few hundred picoseconds equilibrium time was waited for.

3. Thermodynamic and Static Structural Properties

3.1. Density. The systems simulated under constant pressure conditions arrived at densities of 917.4 kg/mol (system 2) and 916.8 kg/mol (system 3), respectively, which is a discrepancy of less than 2% relative to the experimental value of 900 kg/mol for chains of 16 monomer length.[15] The isochoric simulation of system 1 had a pressure of −500 kPa. In *NVT* simulations, a negative pressure of this magnitude means that the system is not exactly at the correct density but would like to contract a little further. As all densities are quite close to the experimental value, which itself is not too certain, since it was determined for a mixture of *cis*- and *trans*-PI, a closer refinement of the force-field parameters was not deemed necessary. The density also depends weakly on the intrachain part of the potential. If the torsion potentials are switched off, the density increases by about 2%, as the chains can pack more effectively (system 1).

3.2. Single Chain Properties. The mean-squared end-to-end distance of the oligomers was measured between the terminating carbons (C_1^{mono1} and C_5^{monon}). The respective result of 5.12 nm^2 corresponds to 0.0075 nm^2 mol/g for the monomer-weight-specific end-to-end distance. The experimental value of 0.0060 nm^2 mol/g per monomer is for a mixture of *trans*- and *cis*-polyisoprene. The experiments are performed doing small-angle neutron scattering in a melt of 7-mers.[29]

The persistence length l_p measures direction correlations of unit vectors along the chain. It is calculated using suitably defined points along the backbone. The function

$$\langle \vec{u}(\vec{r}) \cdot \vec{u}(\vec{r}_0) \rangle = e^{-|\vec{r}-\vec{r}_0|/l_p} \qquad (2)$$

is fitted against the bond correlation. There is some freedom in how to define the tangent vector in an atomistic model. The vectors connecting the C_1 (or the C_2) atoms of adjacent monomers were investigated. Additionally, intramonomer vectors along the double bond and vectors connecting the two end carbons of the same monomer (C_1-C_5) are included. The bond correlation functions are not really exponential (Figure 3), as the interactions are complex and the chains are short. Thus, persistence lengths deduced from the fitting

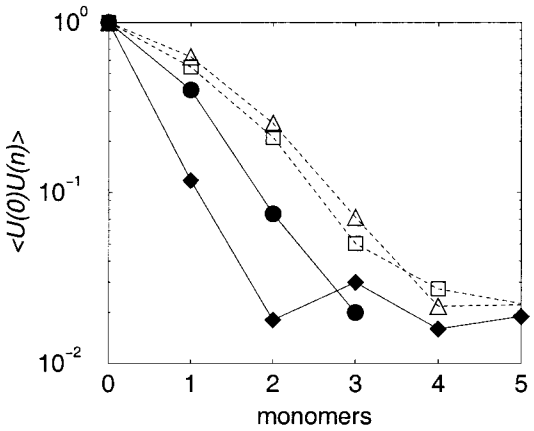

Figure 3. Bond vector correlation functions in the atomistic polyisoprene simulations of system 1. The filled symbols are correlations between direction vectors in the monomers (diamond, double bonds; circle, C_1-C_5). The open symbols correspond to vectors connecting atoms belonging to neighboring monomers (squares, C_2; triangles, C_1).

procedure can only be taken as estimates. End effects were not excluded for reasons of statistics. The correlation functions are different for different vectors. The vector representing the shortest connection (the double bond) has the shortest correlation length. The persistence lengths range between 0.5 (for the double bonds) and 1.5 (for the intermonomer vectors) in monomer diameters (≈0.3 nm). Polyisoprene is, therefore, rather flexible already on the length scale of a few monomers. The monomer itself is intrinsically stiff, but the three torsions between neighboring monomers provide a flexible link.

3.3. Local Packing of Chains. The local structure in the melt can be characterized by different pair distribution functions. Figure 4 shows interchain radial distribution functions of the different atom pairs present in polyisoprene. The curves between the different systems differ only slightly due to density differences. The conspicuous absence of a distinctive first peak in the all-atom and the hydrogen $g(r)$ at short distances indicates that chains cannot easily interpenetrate. Structure is averaged out in the all-atom $g(r)$, in contrast to, e.g., the carbon−carbon distribution function, which exhibits several clear peaks. However, also these do not rise to values $g_{CC}(r) > 1$.

Figure 5 shows the center-of-mass distribution of whole chains. Despite the statistical noise, it is clear that they can approach as close as 0.2 nm. The similarity of the RDFs for systems 2 and 3 suggests that the combination of EBMC and MD leads to a reliable structure. At distances of more than 1 nm the distribution is quite flat; at shorter distances a correlation hole is clearly visible. System 1, which was not equilibrated using the end-bridging, exhibits unrealistically sharp peaks. The differences in the molecular weight distribution also contribute to the different structures. However, molecular dynamics alone is not able to equilibrate a simulation of this size. The introduction of EBMC brings us a good step further, although some remnants of the setup may still be present.

Carbon−carbon radial distribution functions (RDF) resolved according to carbon type allow the study of preferential arrangements between different chains. Partial pair distribution functions between the five different carbons present in polyisoprene were recorded

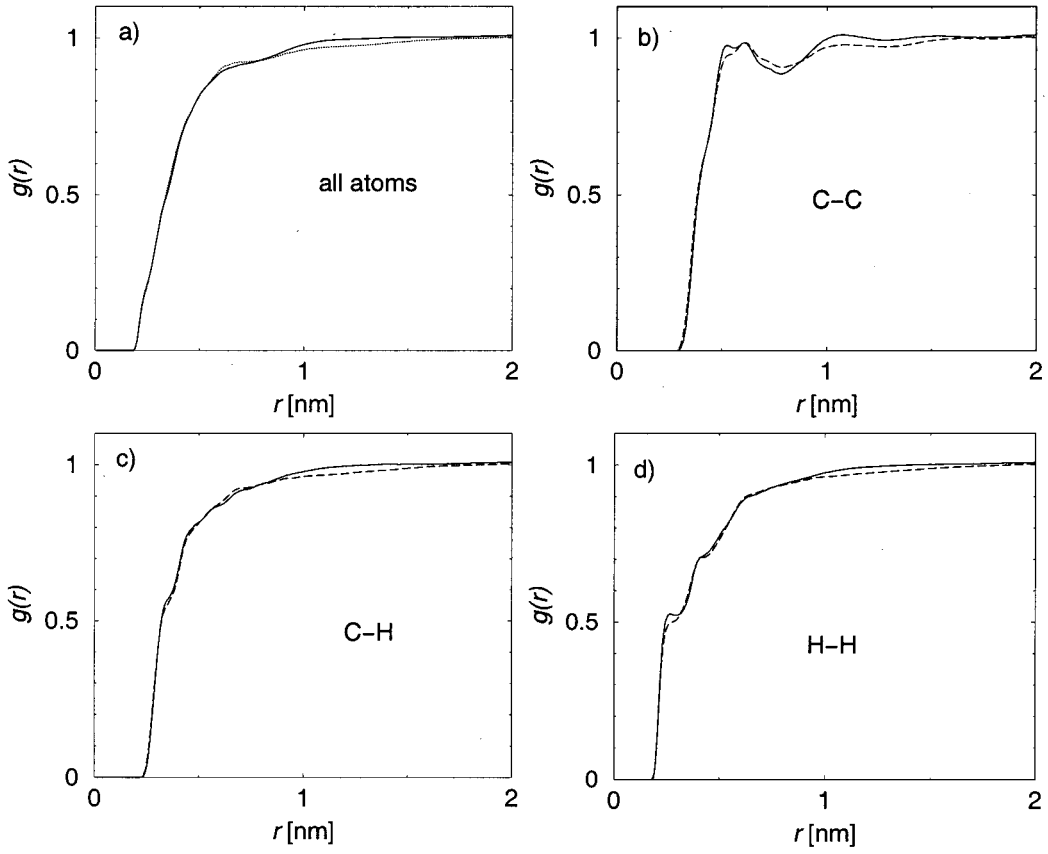

Figure 4. Interchain radial distributions of the different atomic pairs (full line system 1, broken line system 2): (a) all atoms, (b) only carbons, (c) only carbon hydrogen, (d) only hydrogen pairs.

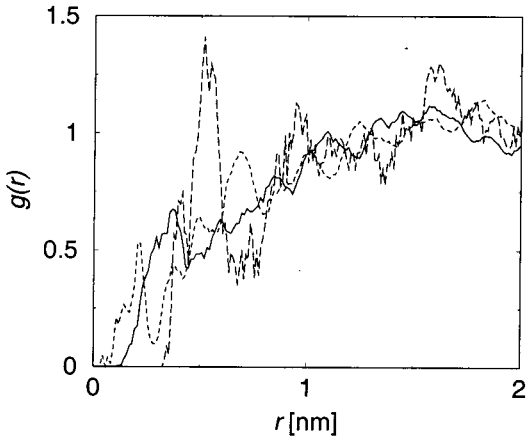

Figure 5. Center-of-mass radial distribution function of the atomistic polyisoprene chains. A correlation hole on local scales is seen; on bigger length scales the distribution is flat. The dashed line corresponds to system 1, the solid line to system 2, and the dotted line to system 3.

(Figure 6). The methyl carbon (C_4) is the most exposed and can, therefore, approach closest to the others (≈0.4 nm). At this distance there is also a shoulder in the C_1, C_2, and C_5 RDF, indicating direct contact. C_3 is the most "shielded" carbon with a slight shoulder at direct contact to C_1. It is linked to C_2, C_4, and C_5; thus, it is often found as second contact (≈0.55 nm). The two methylene carbons C_1 and C_5 are coordinated very similarly. C_2 is easily accessible, as it has only one hydrogen but not very exposed to other chains, since it is part of the double bond in the backbone leading to weak structure.

Integration of the pair distribution function yields the number of neighbors of an atom in a shell of radius r. By relating the local number density $\rho_{\text{local}} = n_C/(4/3)\pi r^3$, n_C being the number of carbons, to the overall concentration $\rho(\infty) = 8.102\ \text{nm}^{-3}$, local enrichment ($x := \rho_{\text{local}}/\rho(\infty) > 1$) and depletion ($x < 1$) can be resolved. Overall integrated values in Figure 6f are smaller than unity due to the correlation hole, as only foreign chains are taken into account. In the innermost shell ($r < 0.45$ nm, cf. Figure 6f) of all carbons methyl groups (C_4) are enriched and sp^2 carbons (C_2 and especially C_3) are depleted, whereas the methylenes (C_1 and C_5) are close in concentration. In the second shell ($0.45 < r < 0.65$ nm), this is partly reversed, as C_3 is enriched and C_4 is weakly depleted. At distances larger than 0.65 nm all species are found at bulk concentration. In brief, one can say that the methylene carbons occur at constant density almost everywhere. The methyl and the double bonded carbons (especially C_3) show much more structure. Monomers of different chains thus approach each other typically with their side groups as closest contact. Orientational influences from the double bond keeping the monomer planar play a role, too (see below). The whole overall structure in the RDFs extends about two monomer sizes ($r < 1$ nm), whereas the concentrations of different carbons level out already at 0.65 nm.

The local structure is not fully described by the (spherically averaged) radial distribution functions. Mutual orientation is measured by the orientation correlation function OCF (Figure 7)

$$\text{OCF}(r) = P_2(r) = \frac{1}{2}\langle 3(\vec{u}_i \cdot \vec{u}_j)^2 - 1\rangle \qquad (3)$$

The distance r is measured between the centers of mass of the respective pairs. Again there are several possible choices for the tangent vectors $\vec{u}_i$. Orientation correlations of the vector connecting the methylenes (C_1-C_5) extend over several interatomic distances (Figure 7a). They resemble the packing of model chains consisting of simple beads.[30] The very few segments that approach closely (cf. Figures 4 and 6) show a perpendicular orientation. A parallel ordering peak is encountered at about 0.4 nm. The first Legendre polynomial ($P_1(r) := \langle \vec{u}_i \cdot \vec{u}_j \rangle$, Figure 7b) which carries direction information shows that these interchain contacts have a small preference of neighboring chains running in the same direction. At larger distances the explicit atomistic structure is no longer important, and the structures become much broader. But there are still structural effects originating from the packing visible up to about 0.7 nm, about two chain diameters.

The order of the double bonds between the chains exhibits more atomistic details. As the double bond leads to a planar configuration of the environment, there is parallel orientation of the neighbors especially at short distances ($r \lesssim 0.4$ nm), which is visible in the first Legendre polynomial. The bond vectors C_5-C_1 (between subsequent monomers), which are about the same length as the double bonds, show even less structure than the simple model.

The intermonomer vectors (Figure 7c), in contrast, display even more generic features which can also be seen in a simple model[3,30,31] (compare section 5). As they describe larger segments compared to the vectors discussed above, the features are less accentuated. On close contact ($r \lesssim 0.4$nm) an almost perfect perpendicular order is found. At intermediate distances (0.4 nm $< r <$ 0.5 nm) a preferred parallel alignment and for the case of the C_2-C_2 vector a second perpendicular region appears ($r \approx 0.8$ nm). The differences between the two different intermonomer (C_1-C_1 and C_2-C_2) vectors are small. So for orientations on length scales as small as monomer sizes, simple models already provide a useful description if the persistence lengths are the same.

This shows that the generic packing effects are important for the understanding of the structure of atomistic models. However, the fine structure at short distances, as found in the first Legendre polynomial, cannot be explained by generic arguments as here the detailed chemistry of the polymer is important.

3.4. Structure of the Melt. Radial distribution functions are quite illustrative in characterizing the structure. However, the experimental observable in scattering experiments is the structure function. The static melt structure factor

$$S_{\text{melt}} = \frac{1}{N}\langle \left| \sum_{m=1}^{N_C} \sum_{j=1}^{N} \exp(i\vec{k}r_j^m) \right|^2 \rangle \qquad (4)$$

is shown in Figure 8 in comparison to simulations of *cis*-polyisoprene[1] and experiments on a mixture dominated by the cis conformer.[10] The melt structure factor shows a clear peak at about 15 nm^{-1}. In addition, there is some smaller structure, especially higher order peaks. The lower limit of resolution is given by the size of the box corresponding to a minimum $|\vec{k}|$ vector of about 0.4π nm^{-1}. At higher temperatures the overall structure flattens out with less pronounced peaks, as expected.

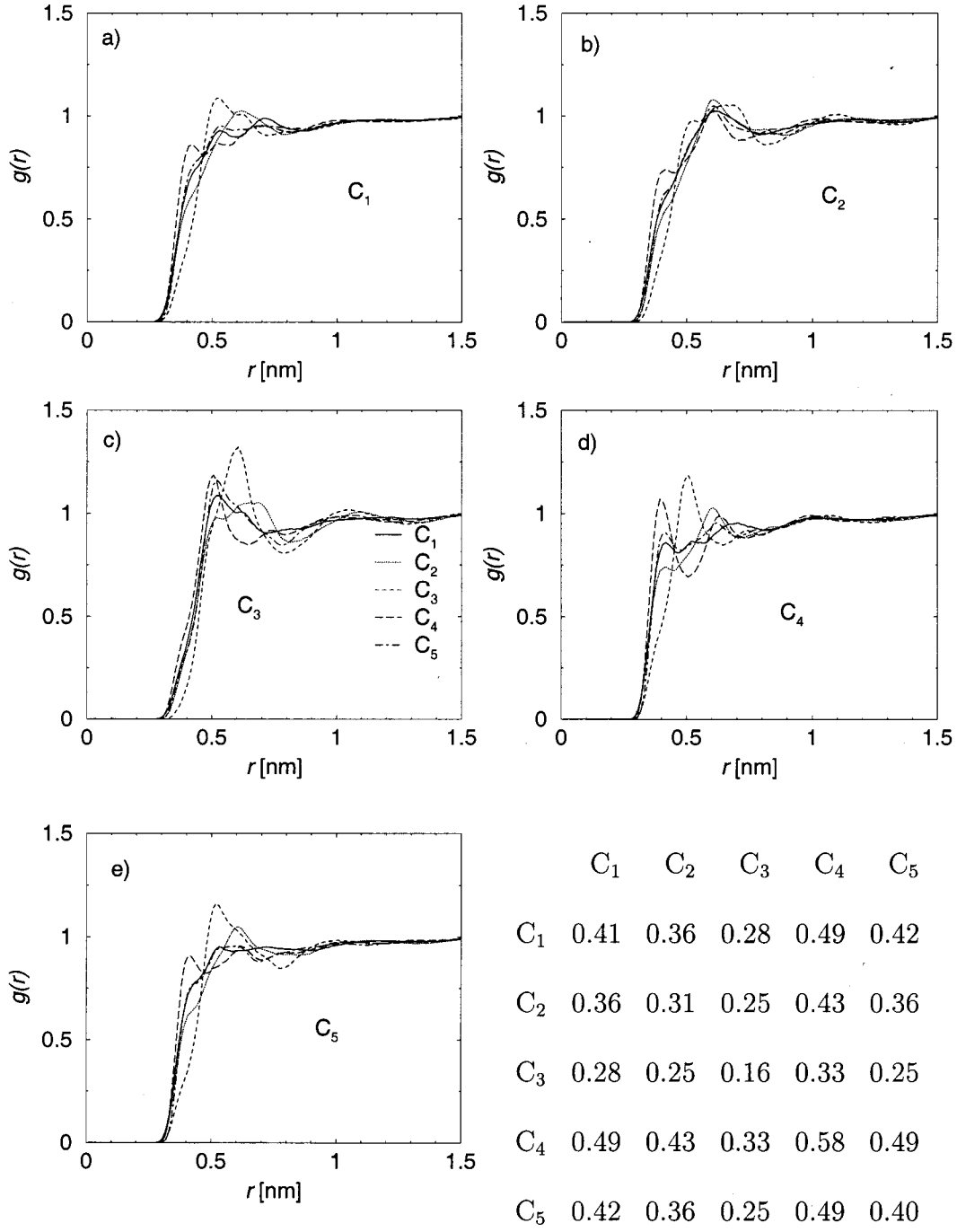

	C_1	C_2	C_3	C_4	C_5
C_1	0.41	0.36	0.28	0.49	0.42
C_2	0.36	0.31	0.25	0.43	0.36
C_3	0.28	0.25	0.16	0.33	0.25
C_4	0.49	0.43	0.33	0.58	0.49
C_5	0.42	0.36	0.25	0.49	0.40

Figure 6. Partial interchain radial distribution functions (system 2, $T = 300$ K): (a) C_1, (b) C_2, (c) C_3, (d) C_4, (e) C_5. In all figures the definition of line styles in (c) applies. (f) (inset table): Integrated number of neighbors in the innermost shell $r < 0.45$nm, only foreign chains.

Moe and Ediger performed simulations on pure *cis*-polyisoprene at 363 and 413 K with one chain of 100 monomers.[1,14] This, obviously, reduces the influence of end effects. The densities were much lower than the experimental values (798 vs 869 and 775 vs 836 kg/m^3, respectively). The structure functions of both simulations are, however, comparable at 413 K. Neither simulation compares really satisfactorily to the experimental structure factor. The double-maximum structure of the first peak is not reproduced, the lower maximum ($\approx$13 nm^{-1}) being enhanced and the higher ($\approx$18 nm^{-1}) being reduced to a shoulder. The positions of the peaks, however, are in reasonable agreement. As the experimental temperature is not given, one cannot say whether at least part of the discrepancy is a low-temperature effect, indicating the formation of a glass, whereas both simulations are performed deep in the melt. Another reason for the disagreement could be the fact that the short chains presented are still oligomers. The alternative would be one long chain, as in refs 14 and 1. However, the periodic boundary replication of a single chain imposes a strong artificial periodicity to a amorphous melt, which makes it difficult to look at *inter*chain effects.

4. Dynamical Properties

4.1. End-to-End Vector. Figure 9 shows for the two polydisperse systems 2 and 3 the reorientation correla-

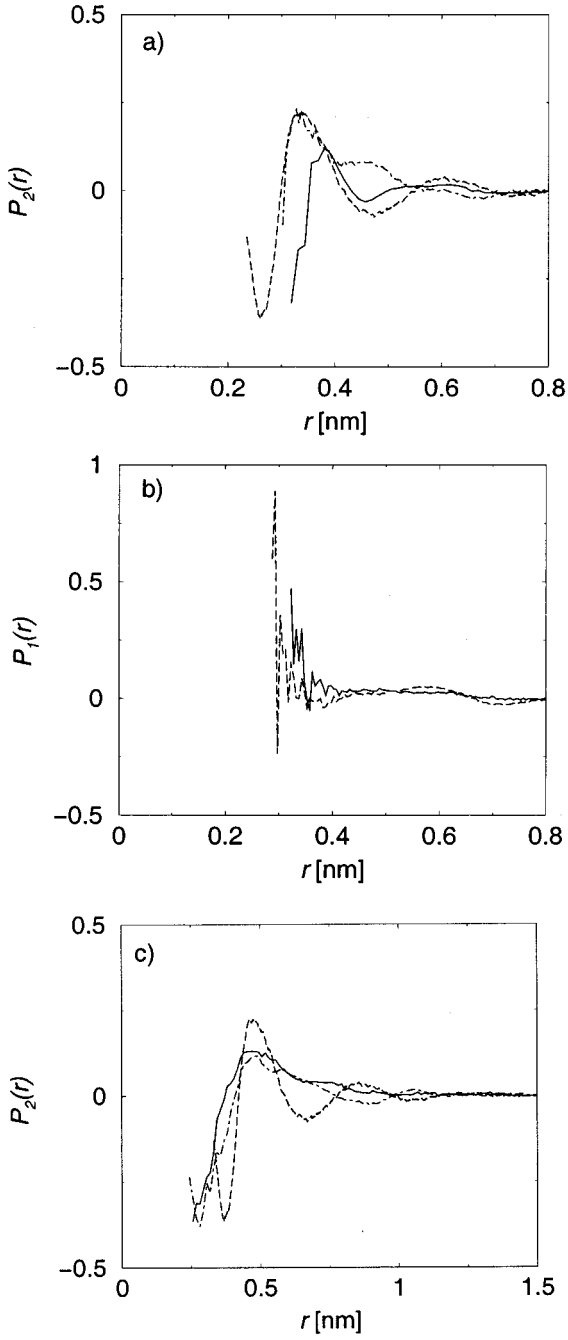

Figure 7. Static *inter*chain orientation correlations OCF (T = 300 K, system 1). (a) Double bonds and vectors connecting C_5 to C_1 of the next monomer between neighboring chains. Dot−dashed: atomistic double bond OCF; solid: C_5-C_1 vectors; dashed: OCF of a simple model with persistence length l_p = 1.5 monomer units[31] scaled for coincidence at the first maximum to the solid one. (b) Same as (a) but P_1 in order to show the directionality of the correlations. (c) Intermonomer vectors, solid line: C_1-C_1; dot−dashed line: C_2-C_2; dashed line: simple model for comparison. Note the different ordinate scale.

tion functions (first and second Legendre polynomial)

$$P_1(t) = \langle(\vec{u}(t)\cdot\vec{u}(0)\rangle \tag{5}$$

$$C_{\text{reor}}(t) := P_2(t) = \langle 0.5[3(\vec{u}(t)\cdot\vec{u}(0))^2 - 1\rangle \tag{6}$$

of the end-to-end vector of the chains of length $N = 10$, which is defined as the vector connecting the two

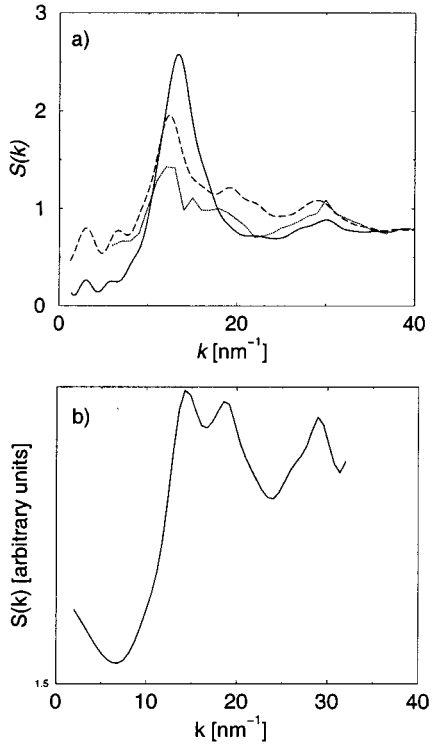

Figure 8. (a) Static structure factor of *trans*-polyisoprene from this work (solid line: T = 300 K; dashed line: T = 413 K) with the scattering lengths of all atoms taken to be the same in comparison to *cis*-PI (dotted line, T = 413 K, data from ref 1). (b) Experimental structure factor obtained by neutron scattering at an unknown temperature at molecular weight of 17 200 (data from ref 10).

terminal carbons C_1^{mono1} and $C_5^{\text{mono}n}$. The relaxation time is clearly longer than the time accessible in the simulations. Even system 2, which was simulated for more than 2 ns, did not relax appreciably on this time scale; local vectors relax, of course, much faster. At the higher temperature of 413 K the relaxation time decreases drastically. Still, one has to be cautious discussing length scales of more than a monomer. This figure shows some scatter between the two systems, which may be taken as a rough estimate of the error of the simulations.

4.2. C−H Bond Reorientation. Reorientation in polyisoprene melts with 92% cis conformer was measured by the group of Lauprêtre and Monnerie.[8,11] Another investigation with a higher trans content of 22%[9] focused also on the cis conformer. Experimentally, the direct observable is the T_1 time.

$$\frac{1}{T_1} = \frac{\hbar^2\gamma_C^2\gamma_H^2}{10r_{C-H}^2}[J(\omega_H - \omega_C) + 3J(\omega_C) + 6J(\omega_H + \omega_C)] \tag{7}$$

The γ_i are the gyromagnetic ratios of the respective nuclei and ω_C and ω_H are the Larmor frequencies, and r is the distance between the nuclei. The function $J(\omega)$ is the spectral density, i.e., the Fourier transform of C_{reor} of the respective C− H vector

$$J(\omega) = \frac{1}{2}\int_{-\infty}^{\infty} C_{\text{reor}}(t)e^{i\omega t}\,dt \tag{8}$$

In atomistic simulations, T_1 has been determined for different polymers.[14,32,33] Moe and Ediger use the limit

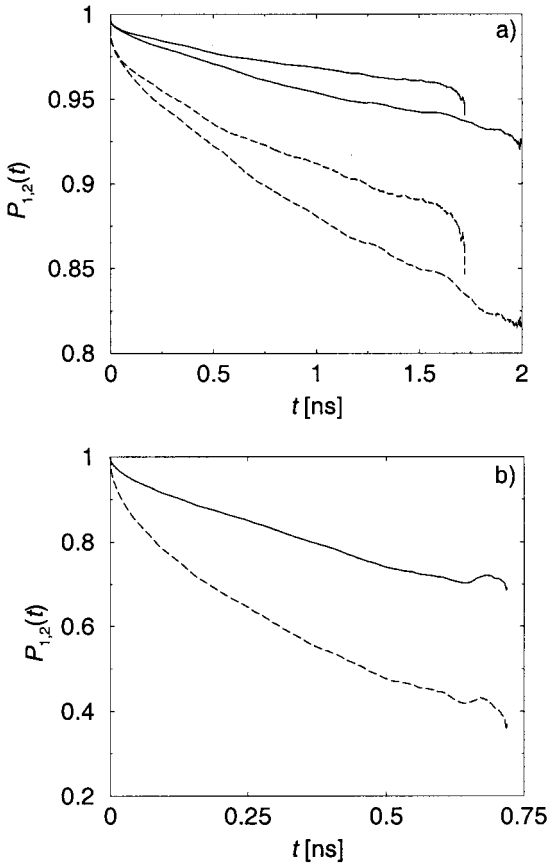

Figure 9. Relaxation of the end-to-end vector. Solid curves are first Legendre polynomials, dashed curves second Legendre polynomials. (a) $T = 300$ K: Of both pairs, the upper curve is the correlation function for system 3 and the lower one for system 2. (b) For $T = 413$ K (system 3) the relaxation times are much shorter.

of *extreme narrowing* ($\omega\tau_{reor} \ll 1$) to analyze their *cis*-polyisoprene data at $T = 413$ K, as is done in most other atomistic simulations.[14] This has the advantage that T_1 becomes independent of the Larmor frequencies,[34] which cannot be measured in simulations without extrapolation. For long chains in a simple model one sees that extrapolation starting at such high values is very questionable.[31] The spectral density $J(\omega)$ is for very short reorientation times independent of ω:

$$J(\omega) = B_{local}^2 \frac{2\tau_{reor}}{1 + \omega^2\tau_{reor}^2} \tag{9}$$

However, the *extreme narrowing* regime is not reached normally by the experiments, as high temperatures are needed to yield correlation times that the results correspond to the limit.

The reorientation time τ_{reor} is defined by the time integral over the correlation function

$$\tau_{reor} = \int_0^\infty C_{reor}\, dt \tag{10}$$

and in the extreme narrowing limit this is directly linked to the T_1 time for a C− H vector

$$T_1^{-1} = 10nK\tau_{reor} \tag{11}$$

where K is a constant related to the bond length and n is the number of protons connected to the respective ^{13}C.

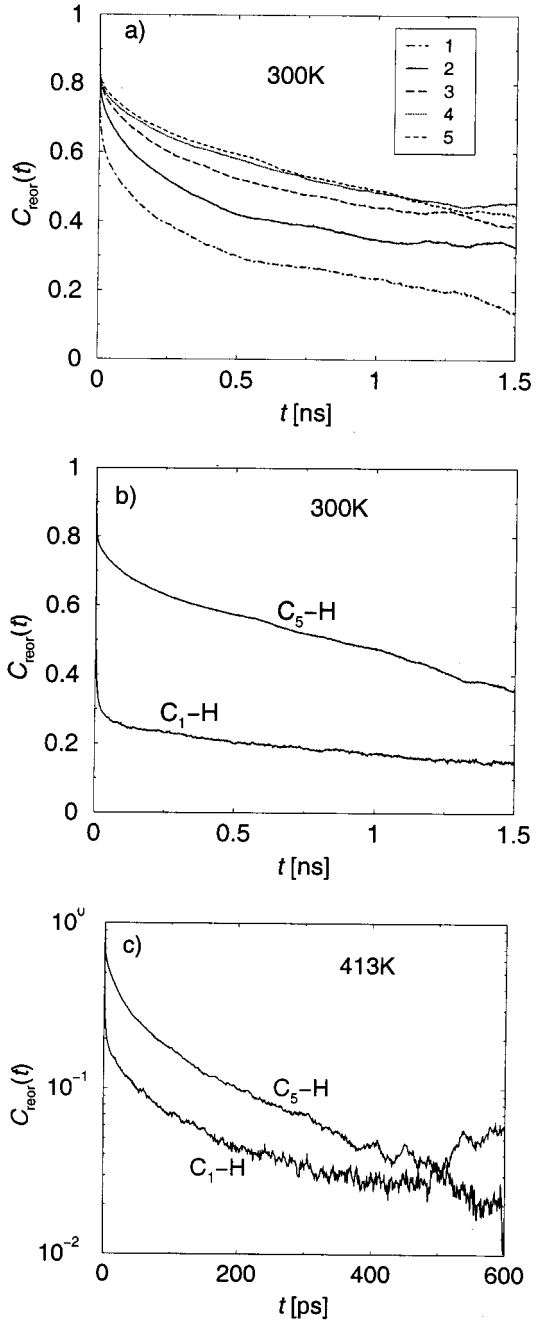

Figure 10. Reorientation of C−H vectors in inner monomers of atomistic polyisoprene chains (system 3, chains of length 10). (a) Vinyl C_2−H depending on monomer position (1: end monomer; 2: next to end monomer; etc.). (b, c) Methylene groups of the central monomer at different temperatures.

Note that a shorter T_1 corresponds to a longer reorientation time.

The C−H vector reorientation is followed in the simulations. To minimize chain-end effects, only the inner-chain monomers are included in Figure 10b,c. Comparing Figures 12a and 10a, one sees that the hydrogen connected to the backbone at carbon C_2 is strongly tied to the backbone. Thus, even such local quantities as bond vectors can be used as observables to monitor the dynamics of intermediate-size chain segments.

Figure 10b illustrates that different torsion potentials and the side group have considerable influence on the reorientation of vectors. The reorientations of the two

Table 7. Comparison of the Experimental (*cis*-PI) and Simulation (*cis*- and *trans*-PI, System 2) Data for the Efficiency of the Initial Stage of the Reorientation Process[a]

	sim: this work		sim: ref 1	exp: ref 8
vector	$a_{\text{fit}}^{\text{trans}}$	$a_{1\text{ ps}}^{\text{trans}}$	$a_{\text{sim}}^{\text{cis}}$	$a_{\text{exp}}^{\text{cis}}$
C_1-H	0.75	0.42	0.28	0.40
C_2-H	0.29	0.16	0.16	0.17
C_5-H	0.29	0.18	0.23	0.48

[a] Fit originates from an exponential fit of the second stage extrapolated to $t = 0$, and $a_{1\text{ ps}}$ is the value of $1 - C_{\text{reor}}$ at 1 ps. In the analysis of the simulations for *cis*-polyisoprene a stretched exponential second process was assumed. The experiments used a range of temperature between 283 and 363 K (ref 8). The trans simulations were at 300 K (this work) and the cis simulations at 363 K (ref 1).

methylene carbons C_1 and C_5 differ. As C_5 is vicinal to the methyl group, the steric hindrance for the hydrogens tied to it is more pronounced. Thus, the initial stage of the reorientation, present for the C_1-H vector, is considerably smaller for C_5-H. This is still visible at 413 K (Figure 10c), although all relaxations are faster. The above-mentioned experiments[8,9] on *cis*-polyisoprene melts show the same tendencies.

Similar to our reorientation correlation function (cf. Figure 10), the experimental data[8] provide evidence for a two-stage process, the first part being simply exponential followed by a nonexponential long-term stage, described by model correlation function

$$C_{\text{reor}}(t) = a\mathrm{e}^{-t\tau_0} + (1-a)\mathrm{e}^{-t/\tau_2}\mathrm{e}^{-t/\tau_1}I_0(t/\tau_1) \quad (12)$$

with τ_0 the local libration time, τ_1 the time of conformation jumps, and τ_2 connected to damping; I_0 is a Bessel function. The separation of time scales for polyisoprene is $\tau_1/\tau_0 \geq 150$ for the two faster characteristic times;[11] the two slow processes (τ_1, τ_2) differ by a factor of 40. A separation of motions was used by Lipari and Szabo as well to analyze NMR data of polymers.[35,36] The correlation function they used has the simpler double-exponential shape

$$C_{\text{reor}}(t) = S^2\mathrm{e}^{-t/\tau_1} + (1-S^2)\mathrm{e}^{-t/\tau_2} \quad (13)$$

where the generalized order parameter S is related to the parameter a of Lauprêtre et al.[11] The reorientation motion is described by one local and one global reorientation if there is no reptation.

Actual numbers for the three times of the model (eq 12) are not provided in refs 8 and 11 but only values for a. Although the experimental polymer is mainly cis, the values for a for the different vectors are comparable between our simulations and experiment (Table 7). The simulation data in our case were determined using a fit to eq 13 with a purely exponential form of the second term, disregarding the Bessel function ($I_0 = 1$). The second column in Table 7 shows the values of a estimated from the value of C_{reor} at 1 ps, which is the shortest time-resolved in the simulations ($a_{1\text{ ps}} = 1 - C_{\text{reor}}(1\text{ ps})$), coming closer to experimental values. This assumes that the first process is too fast to be resolved here. If the conformational jump time is regarded as the time for torsion rearrangement (see below), and keeping in mind that the two times differ at least by a factor of 150, the guess for $a_{1\text{ ps}}$ is probably more realistic. Still, the simulations underestimate the difference between

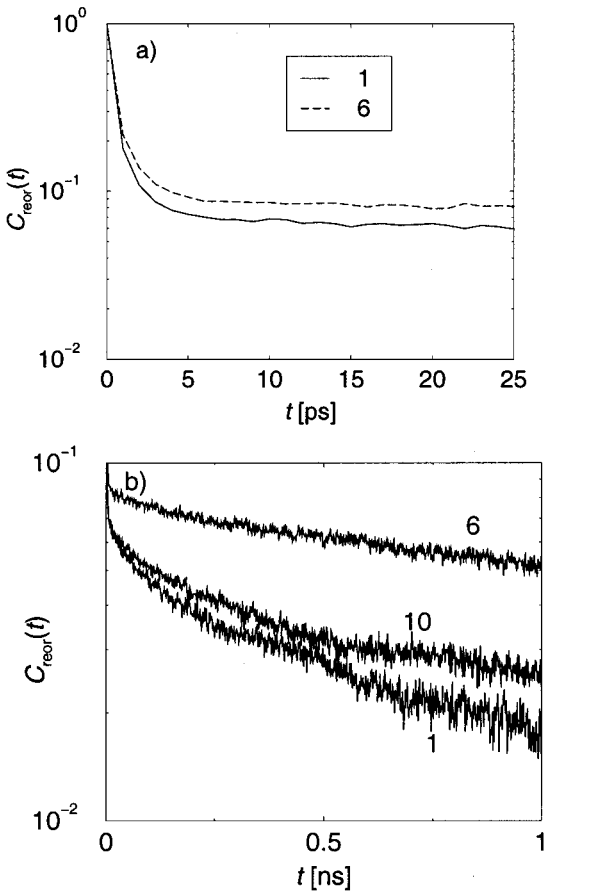

Figure 11. (a) Short time reorientation of methyl C−H vectors, monomer number as in legend (end monomer vs central monomer, system 3, $T = 300$ K, only 10-mers are included). (b) Long time. Clearly, the two stages are separate. A slight difference between the two terminal monomers is visible.

C_1 and C_2 and overestimate the one between C_1 and C_5. The data provided here correspond to a sample of pure *trans*-polyisoprene oligomers which is presumably quite different from real *cis*-polyisoprene with some added trans conformer. Moreover, the discrepancy becomes weaker for system 1 (below). Recent simulations on *cis*-polyisoprene at higher temperature ($T = 363$ K and $T = 413$ K) were interpreted in terms of a two-stage correlation, too. There a separation between the exponential first stage and a stretched exponential second process was deduced.[1] The corresponding a parameters are included in Table 7. Except for the C_5-H vector, they are comparable to our data. For C_5-H they are even farther from the experimental value.

In the reorientation of the C_4-H vectors of the methyl side group the two-stage reorientation is clearly visible (Figure 11a). The first process is nonexponential on the scale of a few picoseconds. The monomer index has almost no influence; only the very local surroundings contribute. On this time scale, the vector does not experience the connection to the chain.

The long time tail, however, is linked to the overall reorientation. The bonding to the chain leads to a bias in the orientation of the methyl group, which prevents total decorrelation on the short time scale. The second (exponential) process is influenced by chain end effects with decay constants of $\tau_{\text{end}} \approx 1$ ns and $\tau_{\text{center}} \approx 3$ ns, respectively (Figure 11b). The decay times were deter-

Table 8. Comparison of Simulated Reorientation Times in *trans*-Polyisoprene (This Work) and *cis*-Polyisoprene (Ref 14) to Data Determined by Extrapolation of Experiments at Lower Temperatures into the Extreme Narrowing Limit[a]

vector	$\tau_{reor}^{trans,sys\ 1}$[ps] 300 K	$\tau_{reor}^{trans,sys\ 2}$[ps] 300 K	$\tau_{reor}^{trans,\ A}$ [ps] 413 K	$\tau_{reor}^{trans,\ B}$ [ps] 413 K	$\tau_{reor}^{(exp)}$ [ps] 413 K	τ_{reor}^{cis} [ps] 413 K
C═C	2400	1900	49	51		
C_1−H	810	640	39	25	22	50
C_2−H	2400	1900	50	46	35	75
C_4−H		480	2.1	5.8	3.6	7.6
C_5−H	1200	1800	67	55	26	60

[a] The cis values[14] were determined by numerical integration of the first 400 ps. For the *trans*-polyisoprene only the two innermost monomers are used. At 413 K the analysis was done in two ways in order to compare more directly to the Moe and Ediger simulations. A: numerical integration and exponential long-time tail (see text). B: Numerical integration to 400 ps. The simulation errors are estimated to be about 20% (difference between systems). The reorientation of the methyl group in the *NVT* simulation could not be calculated meaningfully, as there was a force-field problem. (The hydrogens were connected to the carbon with an additional torsion, which was too strong.)

mined by an exponential fit of the time region between 500 and 1250 ps.

Correlation times for the reorientation of various C−H bonds in *cis*-polyisoprene melts were calculated by Moe and Ediger, who used one long chain under periodic boundary conditions.[14] Table 8 compares the results of this work to their data and the extreme narrowing limit of the experiments. At 300 K, the correlation times were determined by numerical integration of $C_{reor}(t)$ over the first nanosecond and an analytical correction for the exponential tail. For the methyl groups the numerical integration extended only to 20 ps.

Heating to 413 K speeds up the simulation. Here the numerical integration was performed up to 100 ps, again with an analytical correction, except for the methyl groups (20 ps) and the C_1−H (200 ps) (label A in Table 8). For the oligomers, however, the results are very similar to a numerical integration to 400 ps, which was performed additionally in order to compare directly to the data by Moe and Ediger (label B in Table 8).

The discrepancies between the different systems give a measure of uncertainty in the results. The reader is reminded that the systems are governed by slightly differing force fields and are equilibrated in different manners.

If the data are compared directly to extrapolated experimental data, an overall discrepancy of about 50% is found between the trans simulations presented here and the experiments. The integration errors in the simulation as well as the extrapolation of the experiments are sources of error. The systems are not the same, and the simulation model does not reflect reality perfectly. The experiments themselves are not perfectly reliable. Witt et al. showed that NMR experiments for systems as simple as liquid benzene can result in reorientation times differing by an order of magnitude.[37]

In the simulation system 2, the hydrogen at C_5 reflects too much how the backbone reorients on the time scale of the double bond. Experimentally there is a difference between C_5−H and C_2−H. This may result from the interaction with the methyl group which repels the H at C_5 very effectively. In system 1 the difference is more pronounced, as the nonbonded interactions between the methyl hydrogens and the methylene hydrogen are switched off (1−5 interaction, cf. section 2). Comparison with experiment does not allow us to decide which scheme for the exclusion of nonbonded interactions is more appropriate.

4.3. Segmental Motion. The double bonds reflect the reorientation of local segments. The ends reorient faster than inner monomers (Figure 12a); the six innermost monomers are comparable; chains of 10 monomer length have a "bulk" inner part.

There is a two-step reorientation. On very short time scales there is a fast drop due to bond angle vibrations. This is not resolved here. For the inner monomers, a long-time process on the order of the reorientation of the whole chain (a few nano-seconds) sets in afterward.

There is little difference in the dynamics of chains of different lengths, at least in the limited range under study here: the end monomers are free to move regardless of the rest of the chain (Figure 12b), and for central monomers, the relaxation is the same within the (large) statistical error (Figure 12c). As seen in Figure 2, there are very few chains of any length other than 10 in systems 2 and 3.

Denault et al. estimated for chains of molecular weights between 7×10^3 and 1.5×10^5 g/mol a segmental reorientation time of 1.0 ns at 303.15 K and of 43 ps at 373.15 K by analyzing their methylene reorientations.[9] For this, they used the Schaefer model[38] for segmental reorientation, where a χ^2 distribution of relaxation times is assumed, arising from cooperative local motion. The values are of the order of magnitude of the reorientation data presented here for 300 K. However, the chains are clearly longer, and the focus is on the cis conformer. The chain length dependence is weak. An Arrhenius plot of the segmental reorientation time of Denault et al. in comparison to the simulated reorientation of the double bond shows a similar temperature dependence (Figure 13). The activation energies deduced are $E_A^{(sim)} \approx 33$ kJ/mol and $E_A^{(exp)} = 65$ kJ/mol at low temperature and $E_A^{(exp)} = 19$ kJ/mol at high temperature. The effective experimental activation energy taking only the lowest and extrapolated highest point into account arrives at $E_A^{(exp)} \approx 36$ kJ/mol rather close to the simulation value. To decide whether there is a similar behavior as in experiments with two temperature regimes, more simulations at intermediate temperatures would be necessary.

5. Mapping onto a Simple Model

As atomistic models such as the one presented here are obviously too demanding in computer time for long chain and/or long time investigations, mapping onto simpler models is highly desirable. The simple model we choose here is made of soft spheres (repulsive Lennard-Jones potential) connected by anharmonic springs and a weak harmonic bond angle potential leading to a persistence length of 1.5 monomeric units chosen similar to the atomistic model. For details of the model and results on structure and dynamics, see refs 30 and 31.

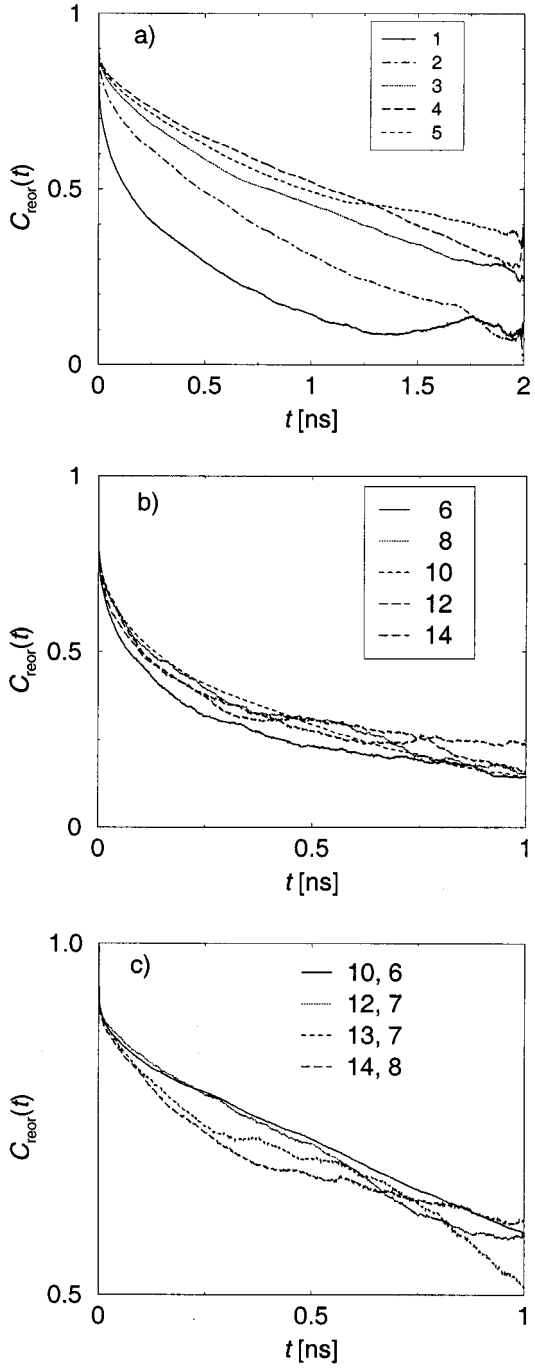

Figure 12. Reorientation of double bonds in system 2 at 300 K: (a) Only the chains with 10 monomers; results shown for different monomer distances from chain end. (b) Only the first monomer for different chain lengths. (c) Central monomers of the chains of length 10 monomers and more (the first number denotes the chain length, the second the monomer number) in semilogarithmic representation.

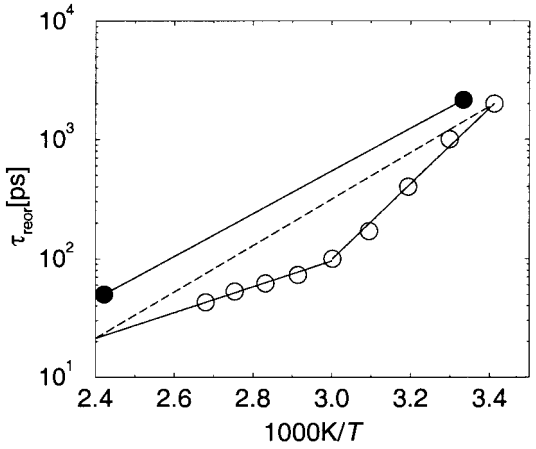

Figure 13. Arrhenius-plot comparing the C=C reorientation time of the simulations (filled circles) to the segmental reorientation time inferred by Denault et al. from their experiments on *cis*-PI at temperatures between 293 and 373 K at molecular weights of 7000 to 130 000.[9] For the simulations the values of Table 8 are averaged at 300 and 413 K, respectively. The solid lines are exponential fits to the curves.

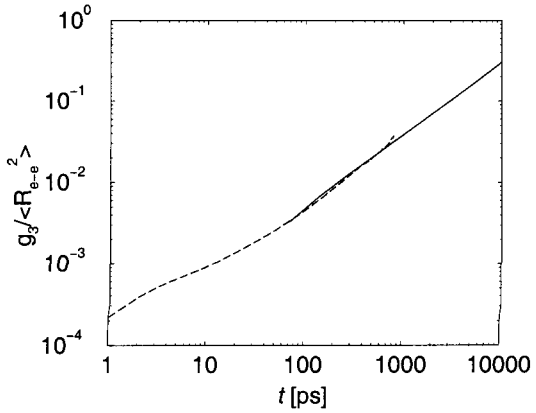

Figure 14. Mean-square displacements of the center-of-mass in the atomistic simulation at 413 K (dashed line) and in the simple model with persistence length 1.5 monomer units (solid line). The ordinates are rescaled by the respective mean-square end-to-end distances. The time scale of the simple model is adjusted to bring the curves into coincidence for a whole order of magnitude.

We have to choose a mapping of one model onto the other before we can compare. For the mapping of length scales the natural choice is the mean end-to-end distance. Thus, melts of 10-mers of the atomistic and the simple models are simulated; then the lengths are set equal. The atomistic simulations of system 3b and simulations presented in ref 31 are used. The convergence of global chain properties in the atomistic case is shown in Figures 9b and 14. For the mapping of time scales a dynamic quantity is necessary. We map in Figure 14 the center-of-mass mean-square displacements $g_3(t)$ onto each other. Because of limited simulation times, a corresponding mapping at 300 K could not be accomplished.

With this mapping fixed, comparative analyses of the two models can be employed in order to check whether both models follow the same dynamics. Figure 15 shows the respective results for the mean-square-displacement of inner monomers, $g_1(t)$, the first three Rouse modes and the reorientation of nearest-neighbor monomer-connecting vectors. These vectors are for the simple model just vectors connecting the beads. For the detailed model, these are vectors connecting the same carbon in adjacent monomers, i.e., C_1-C_1 (dotted line) and C_2-C_2 (dashed line). For the Rouse mode analysis of the atomistic model the centers-of-mass of the double bond are taken as monomer positions. The first three Rouse modes and the inner-monomer MSD do not coincide perfectly within this mapping. Still, they differ by only about a factor of 2−3. The reorientation of the monomer−monomer vector even coincides without any refinement. The two differently defined vectors in the atomistic models are almost indistinguishable. Thus, on this scale

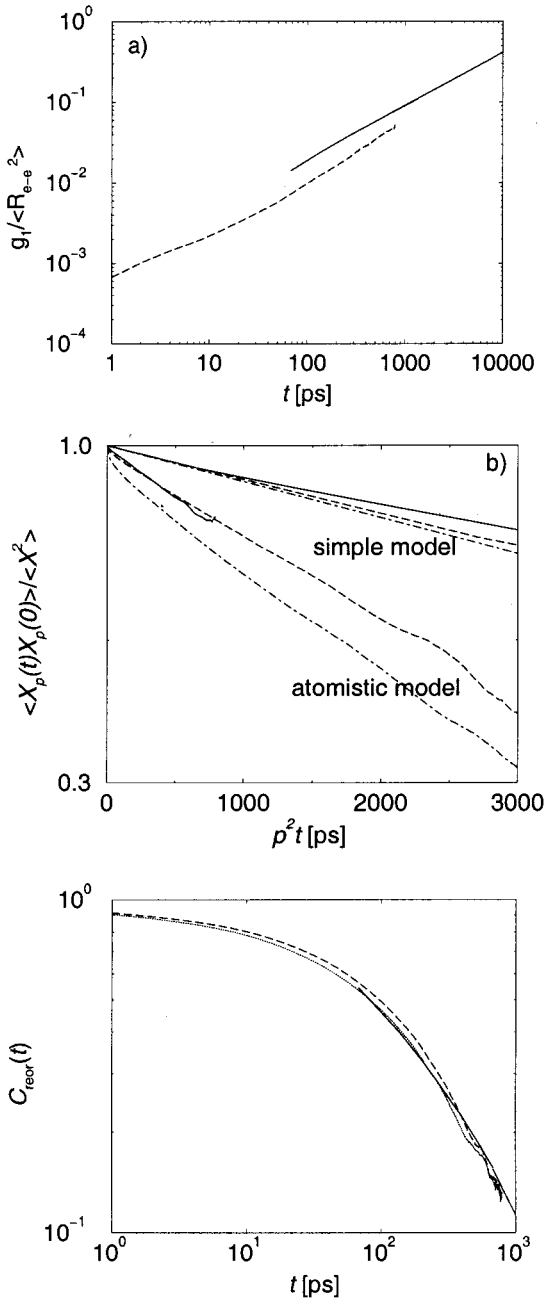

Figure 15. Comparative analysis of the simple model with persistence length $l_p = 1.5$ and the atomistic simulation at $T = 413$ K. (a) Inner monomer mean-square displacement (dashed line: atomistic model; center-of-mass of double bond of central monomer; solid line: simple model). (b) Rouse modes (solid lines: first mode; dashed: second mode; dot−dashed: third mode). (c) Reorientation of nearest-neighbor monomer connecting vectors of the atomistic model at 413 K compared to the simple model.

the atomistic details are already rather unimportant; they may be incorporated into an intrinsic chain stiffness. These results show that the local dynamics are not exactly the same for the atomistic and the simple (coarse-grained) model. There are striking similarities, however, which are much stronger than one might expect as the models are completely different. This finding confirms the concept that the atomistic details on the scale of more than a monomer play only the role of shaping a persistence length. With the simple model we have carried out several investigations,[7,30,31,39] especially of local reorientation.

One might argue that discrepancies of a factor of 3 are no small effects. However, keeping in mind that the two models are drastically different, one would expect on first sight a much stronger discrepancy. We performed the extreme step from the smallest possible model without quantum effects to a model where the complete identity of the polymer is only regarded by means of its stiffness.The successful mapping to the atomistic model is a further (retrospective) validation of those results. A more detailed investigation of the mapping will be shown in a separate publication.[40]

6. Conclusions

This simulation study is concerned with decamers of *trans*-polyisoprene, which are short in comparison to experimental systems. Yet, the simulations are able to describe correctly local structural and dynamical features of the polymer. This can be seen by comparing results like chain extension, structure functions, and correlation times for C−H vectors obtained by NMR. Taking into account that the simulated and experimental systems are not always identical in composition, temperature, and so on, the agreement is quite good. We have also recently studied the free volume properties of our melts and compared them to positronium annihilation data,[41] and the agreement is again very good. We thus conclude that our all-atom model provides a faithful description of this polymer.

With the model, we analyzed the packing of chains. The detailed analysis of several interchain radial distribution functions shows that monomers approach each other most strongly with the exposed methyl groups followed by the methylene groups, whereas the vinyl carbons tend to be less accessible. All specificity in the interaction is however limited to the first solution shell. This is also seen in the mutual orientation of tangent vectors of neighboring chains. Chains have the tendency to be parallel at the first-neighbor distance. The orientational correlation between second neighbors is already very small. From comparing different choices for the tangent vectors it is also evident that the orientations of bond vectors (i.e., short vectors) show some structure arising from atomistic interactions, whereas the orientation between intermonomer (long) vectors is less structured and already close to what is found for a generic bead−spring model.[30,39]

The reorientation dynamics of bond (C−C and C−H) vectors typically follows a two-stage process: a fast (picosecond) relaxation due to local vibrations followed by a long-time reorientation characteristic for the reorientation of the parent polymer segment. The relative contribution of both processes to the overall reorientation is in good agreement with estimates from NMR measurements.

To study the nonlocal structure and dynamics of *trans*-polyisoprene, extensive simulations have been performed with a generic bead−spring model which was only augmented by an intrinsic bending stiffness.[7,31] We have successfully mapped this model onto the present atomistic simulation. After matching length and time scales, all characteristic time constants then agree to within a factor of 2−3. This illustrates that it is possible to develop polymer models at different levels of detail and have a description of polymer dynamics which smoothly connects both time scales. Systematic protocols for mapping atomistic to coarse-grained models and back are therefore being developed in our laboratory also for other polymer systems.[42−45]

An interesting technical point is the comparison between the polymer samples equilibrated with end-bridging Monte Carlo (EBMC) and those without. The EBMC proves to be a useful tool in the initial equilibration of polymer melts as it offers a way to wander through phase space more efficiently. At a global structural level, the EBMC provides better equilibrated samples. However, it is quite surprising that strictly local properties like monomer packing or bond-vector reorientation do not seem to be affected appreciably by the way the sample is prepared.

Acknowledgment. We thank Kurt Kremer and Heiko Schmitz for fruitful discussions. Financial support from the German ministry of research (BMBF) as well as the TMR program of the European Union (Contract Number CRBFMRXCT980176) is gratefully acknowledged.

References and Notes

(1) Moe, N. E.; Ediger, M. D. *Phys. Rev. E* **1999**, *59*, 623−630.
(2) Schmitz, H.; Müller-Plathe, F. *J. Chem. Phys.* **2000**, *112*, 1040−1045.
(3) Müller-Plathe, F.; Schmitz, H.; Faller, R. *Prog. Theor. Phys. (Kyoto) Suppl.* **2000**, *138*, 311−319.
(4) Grest, G. S.; Kremer, K. *Phys. Rev. A* **1986**, *33*, R3628−R3631.
(5) van Gunsteren, W. F.; Berendsen, H. J. C. *Angew. Chem., Int. Ed. Engl.* **1990**, *29*, 992−1023.
(6) Kremer, K.; Grest, G. S. *J. Chem. Phys.* **1990**, *92*, 5057−5086.
(7) Faller, R.; Müller-Plathe, F. *Chem. Phys. Chem.*, in press.
(8) Dejean de la Batie, R.; Lauprêtre, F.; Monnerie, L. *Macromolecules* **1989**, *22*, 122−129.
(9) Denault, J.; Prud'homme, J. *Macromolecules* **1989**, *22*, 1307−1316.
(10) Zorn, R.; Richter, D.; Farago, B.; Frick, B.; Kremer, F.; Kirst, U.; Fetters, L. J. *Physica B* **1992**, *180&181*, 534−536.
(11) Lauprêtre, F.; Bokobza, L.; Monnerie, L. *Polymer* **1993**, *34*, 468−475.
(12) Dlubek, G.; Fretwell, H. M.; Alam, A. *Phys. Status Solidi A* **1998**, *167*, R13−R14.
(13) English, A. D.; Ingfield, P. T.; Jones, A. A.; Zhu, Y. *Polymer* **1998**, *39*, 309−313.
(14) Moe, N. E.; Ediger, M. D. *Polymer* **1996**, *37*, 1787−1795.
(15) Fetters, L. J.; Lohse, D. J.; Graessley, W. W. *J. Polym. Sci., Part B: Polym. Phys.* **1999**, *37*, 1023−1033.
(16) Pant, P. V. K.; Theodorou, D. N. *Macromolecules* **1995**, *28*, 7224−7234.
(17) Mavrantzas, V. G.; Boone, T. D.; Zervopoulou, E.; Theodorou, D. N. *Macromolecules* **1999**, *32*, 5072−5096.
(18) Frisch, M. J.; Trucks, G. W.; Schlegel, H. B.; Gill, P. M. W.; Johnson, B. G.; Robb, M. A.; Cheeseman, J. R.; Keith, T. A.; Petersson, G. A.; Montgomery, J. A.; Raghavachari, K.; Al-Laham, M. A.; Zakrzewski, V. G.; Ortiz, J. V.; Foresman, J. B.; Cioslowski, J.; Stefanov, B. B.; Nanayakkara, A.; Challacombe, M.; Peng, C. Y.; Ayala, P. Y.; Chen, W.; Wong, M. W.; Andres, J. L.; Replogle, E. S.; Gomperts, R.; Martin, R. L.; Fox, D. J.; Binkley, J. S.; Defrees, D. J.; Baker, J.; Stewart, J. P.; Head-Gordon, M.; Gonzalez, C.; Pople, J. A. *Gaussian 94 Revision C.3*; Gaussian, Inc.; Pittsburgh, PA, 1995.
(19) Frisch, M. J.; Trucks, G. W.; Schlegel, H. B.; Scuseria, G. E.; Robb, M. A.; Cheeseman, J. R.; Zakrzewski, V. G.; Montgomery, J. A.; Stratmann, R. E.; Burant, J. C.; Dapprich, S.; Millam, J. M.; Daniels, A. D.; Nudin, K. N.; Strain, M. C.; Farkas, O.; Tomasi, J.; Barone, V.; Cossi, M.; Cammi, R.; Menucci, B.; Pomelli, C.; Adamo, C.; Clifford, S.; Ochterski, J.; Petersson, G. A.; Ayala, P. Y.; Cui, Q.; Morokuma, K.; Malick, D. K.; Rabuck, A. D.; Raghavachari, K.; Foresman, J. B.; Cioslowski, J.; Ortiz, J. V.; Stefanov, B. B.; Liu, G.; Liashenko, A.; Piskorz, P.; Komaromi, I.; Gomperts, R.; Martin, R. L.; Fox, D. J.; Keith, T.; Al-Laham, M. A.; Peng, C. Y.; Nanayakkara, A.; Gonzalez, C.; Challacombe, M.; Gill, P. M. W.; Johnson, B. G.; Chen, W.; Wong, M. W.; Andres, J. L.; Head-Gordon, M.; Replogle, E. S.; Pople, J. A. *Gaussian 98 Revision A.5*; Gaussian, Inc.; Pittsburgh, PA, 1998.
(20) Becke, A. D. *J. Chem. Phys.* **1993**, *98*, 5648−5652.
(21) Faller, R.; Schmitz, H.; Biermann, O.; Müller-Plathe, F. *J. Comput. Chem.* **1999**, *20*, 1009−1017.
(22) Schmitz, H.; Faller, R.; Müller-Plathe, F. *J. Phys. Chem. B* **1999**, *103*, 9731−9737.
(23) Faller, R. Influence of Chain Stiffness on Structure and Dynamics of Polymers in the Melt. Ph.D. Thesis, MPI für Polymerforschung and Universität Mainz, 2000; published at http://archimed.uni-mainz.de/pub/2000/0063.
(24) Allen, M. P.; Tildesley, D. J. *Computer Simulation of Liquids*; Clarendon Press: Oxford, 1987.
(25) Berendsen, H. J. C.; Postma, J. P. M.; van Gunsteren, W. F.; DiNola, A.; Haak, J. R. *J. Chem. Phys.* **1984**, *81*, 3684−3690.
(26) Müller-Plathe, F. *Comput. Phys. Commun.* **1993**, *78*, 77−94.
(27) Ryckaert, J.-P.; Cicotti, G.; Berendsen, H. J. C. *J. Comput. Phys.* **1977**, *23*, 327−341.
(28) Müller-Plathe, F.; Brown, D. *Comput. Phys. Commun.* **1991**, *64*, 7−14.
(29) Fetters, L. J.; Lohse, D. J.; Richter, D.; Witten, T. A.; Zirkel, A. *Macromolecules* **1994**, *27*, 4639−4646.
(30) Faller, R.; Kolb, A.; Müller-Plathe, F. *Phys. Chem. Chem. Phys.* **1999**, *1*, 2071−2076.
(31) Faller, R.; Müller-Plathe, F.; Heuer, A. *Macromolecules* **2000**, *33*, 6602−6610.
(32) Paul, W.; Smith, G. D.; Yoon, D. Y. *Macromolecules* **1997**, *30*, 7772−7780.
(33) Antoniadis, S. J.; Samara, C. T.; Theodorou, D. N. *Macromolecules* **1998**, *31*, 7944−7952.
(34) Kalinowski, H.-O.; Berger, S.; Braun, S. *^{13}C NMR-Spektroskopie*; Thieme; Stuttgart, 1984.
(35) Lipari, G.; Szabo, A. *J. Am. Chem. Soc.* **1982**, *104*, 4546−4559.
(36) Lipari, G.; Szabo, A. *J. Am. Chem. Soc.* **1982**, *104*, 4559−4570.
(37) Witt, R.; Sturz, L.; Dölle, A.; Müller-Plathe, F. *J. Phys. Chem. A* **2000**, *104*, 5716−5725.
(38) Schaefer, J. *Macromolecules* **1973**, *6*, 882−888.
(39) Faller, R.; Pütz, M.; Müller-Plathe, F. *Int J. Mod. Phys. C* **1999**, *10*, 355−360.
(40) Faller, R.; Müller-Plathe, F. *Comput. Theor. Polym. Sci.*, in press.
(41) Schmitz, H.; Müller-Plathe, F.; Faller, R. Manuscript in preparation.
(42) Tschöp, W.; Kremer, K.; Batoulis, J.; Bürger, T.; Hahn, O. *Acta Polym.* **1998**, *49*, 61−74.
(43) Tschöp, W.; Kremer, K.; Hahn, O.; Batoulis, J.; Bürger, T. *Acta Polym.* **1998**, *49*, 75−79.
(44) Meyer, H.; Biermann, O.; Faller, R.; Reith, D.; Müller-Plathe, F. *J. Chem. Phys.* **2000**, *113*, 6264−6275.
(45) Reith, D.; Meyer, H.; Müller-Plathe, F. *Macromolecules*, in press.
(46) Lide, D. R., Ed.; *CRC Handbook of Chemistry and Physics*, 76th ed.; CRC Press: Boca Raton, FL, 1995.

MA0016782